Symmetric mass and temporally unbounded quantum gravity solution in causal dynamical triangulations

Kyle Lee*
Schmid College of Science
Chapman University
Orange, CA 92866

Abstract

In this paper, we demonstrate how one of the fixed-boundary causal dynamical triangulations simulation returns a numerical result that resembles the geometry of Lorentzian de Sitter space, signaling a first discovery of temporally unbounded quantum gravity solution in causal dynamical triangulations. We also discuss how we can create a causal dynamical triangulations simulation with a mass simplex, and raise some of the issues that we are faced with; we explain some of our latest results and future plans on creating a complete model with a mass simplex.

1 Introduction

Quantum gravity is a theory that is expected to reconcile quantum mechanics and general relativity. Despite strenuous efforts of many researchers, such theory has proved to be very elusive to find, and lack of direct experimental data in the realm of quantum gravity may inspire one to question the practicality and even the existence of such theory. Despite all, however, quantum gravity is expected to give insight to many fundamental questions related to black hole's singularity and event horizons, cosmological beginning, information paradox, and more. Its existence is theoretically expected and search for the theory of quantum gravity is truly at the culmination of human endeavor to understand the workings of the universe [8].

One of the difficulties of quantum gravity comes from the breakdown of perturbative theory at high energy; causal dynamical triangulations (CDT) is a nonperturbative formulation of quantum gravity which uses Wilsonian approach of adjusting bare coupling constants to arrive at a meaningful results [2].

Two things that is expected from any successful theory of quantum gravity are: 1) It has to reproduce any of the experimentally verified semi-classical results at an appropriate limits and 2) It must produce novel quantum mechanical phenomena (or else, there is no reason to consider it). CDT has so far proved to satisfy both of these vital categories.

In this paper, section 2 will discuss basic formalism of CDT, section 3 will discuss some of the important previous results coming from CDT, section 4 will discuss possible discovery of temporally unbounded quantum spacetime geometry in CDT, and section 5 will discuss CDT solution with symmetric mass.

*lee603@mail.chapman.edu

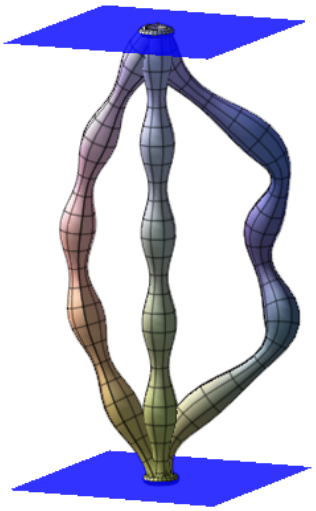

(a) Different spacetime histories with common boundary geometry.

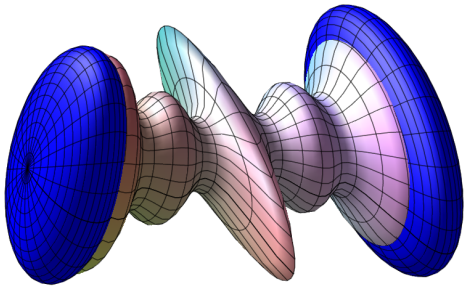

(b) One particular spacetime history with a fixed boundary geometry.

Figure 2.1: Evaluation of path integral involves summing over all spacetime histories with common boundary geometry. Images by J. Miller

2 Basics of Causal Dynamical Triangulations

2.1 Path Integration Approach

Path integral quantization scheme uses Lagrangian, as oppose to Hamiltonian as in canonical quantization scheme. Using the appropriate Lagrangian related to the dynamical variable one is quantizing, one can compute actions for various paths with common initial and final boundary conditions of the dynamical variable. For instance, if we are quantizing the path of classical particle with initial point(t_0, x_0) and final point(t_1, x_1), we must evaluate the path integral[1],

$$P(x_0(t_0), x_1(t_1)) = \int_{x_0}^{x_1} [\mathscr{D}x(t)] e^{iS[x(t)]/\hbar} \tag{1}$$

where $\int_{x_0}^{x_1}[\mathscr{D}x(t)]$ is a symbolic way of saying integrate over all the paths connecting x_0 and x_1 at t_0 and t_1, respectively. To quantize gravity, we take the spacetime metric, g, to be the dynamical variable which we are quantizing. If we have manifold $\mathscr{M}$, the path integral would be defined as,

$$P(\gamma) = \int_{g|\partial\mathscr{M}=\gamma} [\mathscr{D}g] e^{iS[g]} \tag{2}$$

where $\partial\mathscr{M}$ represents the boundary of the manifold $\mathscr{M}$, and γ and g represent metric tensors of the $\partial\mathscr{M}$ and $\mathscr{M}$, respectively.[2] Also, $S[g]$ includes Einstein-Hilbert action, $S_{EH}[g] = \frac{1}{16\pi G}\int_{\mathscr{M}} d^{(d+1)}\sqrt{-g}(R-2\Lambda)$ where R is the Ricci scalar and Λ is the cosmological constant, and Gibbons-Hawking-York boundary term, $S_{GHY}[g] = \frac{1}{8\pi G}\int_{\partial\mathscr{M}} d^d y\sqrt{|\gamma|}K$ where γ is the determinant of the induced metric on the boundary $\partial\mathscr{M}$ and K is the extrinsic curvature of the boundary

[1] Unlike in a classical theory, what we get is not a true physical path that particle takes, but rather a transition amplitude.

[2] we integrate over only physically distinct histories, i.e. distinct g upto diffeomorphism

$\partial\mathscr{M}$. However, evaluating this integral with all possible continuous spacetime histories with appropriate boundary conditions is hopelessly difficult and the integral is also divergent [8]. To resolve this issue, we discretize spacetime by coordinate-independent Regge Calculus representation [6]. Regge Calculus representation discretizes spacetime by introducing UV-cutoff length 'a', thus resolving the issue of divergence. Regge's formulation uses triangulation technique of the manifold by simplices. Such triangulations create piecewise linear geometries of spacetime where curvatures are concentrated in $(n-2)$-dimensional simplices of the (n)-dimensional manifold being triangulated, and edge lengths and number of simplices used for triangulations can be appropriately adjusted to gain different levels of approximation of the manifold.

The (2) now becomes a discrete sum,

$$P[\partial\mathcal{T}] = \sum_{\mathcal{T}} \frac{1}{\mu(\mathcal{T})} e^{iS^{(R)}[\mathcal{T}]} \tag{3}$$

where sum is over all piecewise linear geometries by triangulation, $\mathcal{T}$, with common boundary geometry, $\partial\mathcal{T}$. Also, $\mu(\mathcal{T})$ is the order of the automorphism group of the triangulation $\mathcal{T}$. One might naively expect to consider all the Lorentzian triangulation with appropriate boundary conditions, however, the complex weight of the sum makes numerical evaluation of the sum difficult. Thus, we want to somehow turn this complex weight to a real weight, which can be done using a Wick rotation to Euclidean space. This turns the path integral sum into a partition function,

$$Z[\partial\mathcal{T}] = \sum_{\mathcal{T}} \frac{1}{\mu(\mathcal{T})} e^{-S^{(E)}[\mathcal{T}]} \tag{4}$$

with familiar Boltzmann weight and partition function from statistical physics. Therefore, we can intuitively think of geometry taking certain triangulation with probability $e^{-S[\mathcal{T}]}$.[3] However, not any Lorentzian triangulation can be Wick rotated to Euclidean triangulation in general. It was proposed by Ambjørn and Loll to consider only the Lorentzian triangulation with well-defined causal structures, which has a well defined Wick rotation.[4]

2.2 Causal Structures

A Lorentzian triangulation with causal structure is simply geometries with time foliations, which means $(d+1)$-dimensional manifold can be represented by $\mathscr{M} = I \times \Sigma$, where Σ is (d)-dimensional spacelike hypersurface and I represent proper time interval.[5] The most common choice of Σ for CDT is S^{d-1}. S^2 can be triangulated, for instance, by patching four triangles (which is minimum number of triangles needed to triangulate S^2) along its faces as figure 2.2 shows. In general, (n)-dimensional manifold is triangulated by (n)-dimensional simplices. In CDT, we initialize the simulation with minimal triangulation of each spacelike hypersurface (or time slice) with (d)-dimensional simplices. Then, adjacent time slices are connected by timelike edges to form $(d+1)$-dimensional simplices and complete triangulation of the manifold $\mathscr{M}$.

[3] This is convenient way to imagine which triangulations are most important in evaluating the partition sum and it matches our intuition from statistical physics; however, this is not true in the sence of path integral since a single path is not a quantum observable.

[4] This proposal is not just a blind proposal to make the evaluation of the sum (4) possible. Before CDT, there was Euclidean dynamical triangulations, which attempted evaluating (4) by considering all Euclidean piecewise linear geometries, which ended up giving crumpled phase and branched polymer phase, but no phase with extended geometries expected from semiclassical limit. Ambjørn and Loll proposed causal structure as the solution to this issue.

[5] This does not mean we are making a gauge choice, since Regge Calculus representation does not have a coordinate to begin with.

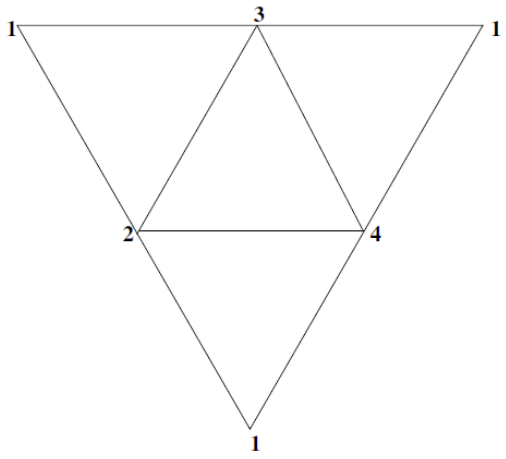

Figure 2.2: A minimal triangulation of a 2-sphere. Image from [7].

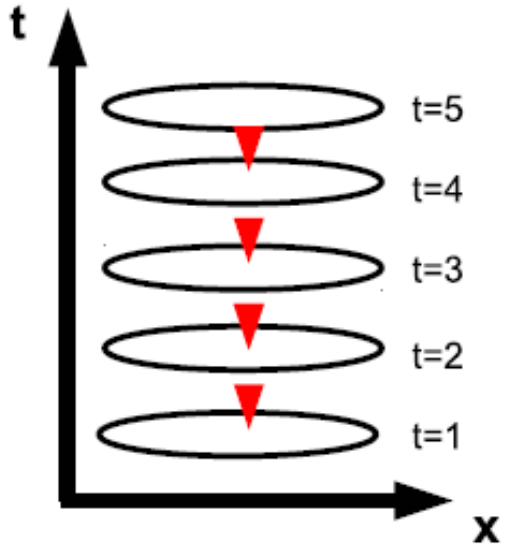

Figure 2.3: A time foliation of spacetime. Image from [16].

All the links (2-dimensional simplex) in the spacelike hypersurface are spacelike with its squared norm a^2, and the timelike links that connect adjacent time slices have squared norm $-\alpha a^2$ with $\alpha > 0$.

2.3 Building Blocks

When we triangulate the $(d+1)$-dimensional manifold $\mathscr{M}$, we get different flavors of $(d+1)$-dimensional simplices. Different types of simplices are labeled by ordered pair (n_0, n_1) where n_0 and n_1 represent number of vertices of the simplex in lower and upper time slices with $n_0 + n_1 = d + 2$. Therefore, we have $(d + 2 - n, n)$ types of simplices where $n = 1, ..., d + 1$.[6] Also, $(d + 2 - n, n)$ and $(n, d + 2 - n)$ are just inverted version of each other. For instance, $(3 + 1)$-spacetime have (4,1), (1,4), (3,2), and (2,3) simplices.

2.4 Pachner Moves

To move through the space of piecewise linear geometries, we have to have a way of going from one triangulation to another. Pachner move changes a given triangulation to another triangulation by changing a configuration of simplicial complex it acts on. (a, b)- pachner move acts on 'a' $(d+1)$-dimensional simplices to produce 'b' $(d+1)$-dimensional simplices. Although it is not rigorously proven for $(3+1)$ case, these moves are assumed to satisfy ergodicity theorem, which is essential for monte carlo algorithms, the numerical algorithm we use in simulation, to be valid; therefore, pachner moves are also known as ergodic moves. The figure 2.4 shows the moves in $(3 + 1)$ case, which has (2,8), (8,2), (4,6), (6,4), (2,4) version 1, (2,4) version 2, (3,3) version 1, and (3,3) version 2 moves. For details of how these moves change the configurations of simplices, refer to [7][2][3]. Regge himself envisioned getting different triangulations by adjusting the edge lengths, however, we rather fix these edge length and arrive at different triangulations by changing the connectivity information (number of different types of simplicies and subsimplices).

[6] Since there cannot be $(d+1)$-dimensional spacelike simplex, $n \neq 0$ and $d + 2$

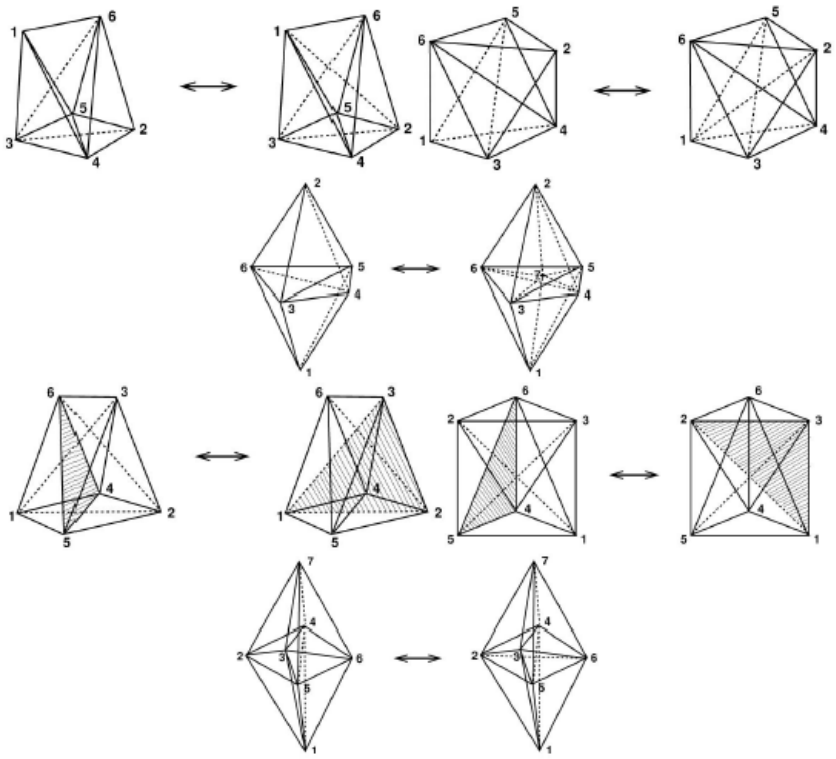

Figure 2.4: Pachner Moves in $(3+1)$-dimensions. Image from [2].

2.5 Metropolis Algorithm

Although there are much more simulation details to be explained, simply put, to generate different triangulations, a simplex and a pachner move is picked out randomly. If making the chosen random move on the chosen random simplex does not violate any constraints, the move might be carried out. To determine whether a certain move is carried out or not, we use metropolis algorithm (as it was pointed out earlier, we can think of each triangulation having a Boltzman probabilistic weight associated with it),

$$P(\mathcal{T}_1 \to \mathcal{T}_2) = \begin{cases} e^{-\Delta S_E} & \text{if } e^{-\Delta S_E} > 0 \\ 1 & \text{if } e^{-\Delta S_E} \leq 0 \end{cases} \tag{5}$$

where $P(\mathcal{T}_i \to \mathcal{T}_j)$ represents the transition probability of going from triangulation $\mathcal{T}_i$ to $\mathcal{T}_j$ and ΔS_E represents the change in the (Euclidean) action values. Thus, we always accept the pachner move if the new triangulation has a higher probability of occurring than the old triangulation. If the new triangulation has a lower probability of occuring than the old triangulation, we accept the pachner move with the probability $e^{-\Delta S_E}$. Therefore, it becomes necessary to evaluate the action in discrete setting. This implies we have to find a discrete representation of $S[g] = S_{EH} + S_{GHY}$ into $S^{(R)}[\mathcal{T}]$, and then take Wick rotation of it to Euclidean action.

Regge himself demonstrated that for a triangulation $\mathcal{T}$, Einstein-Hilbert action assumes the form

$$S^{(R)}_{EH}[\mathcal{T}] = \frac{1}{8\pi G} \sum_{h \in \mathcal{T}} V_h \delta_h - \frac{\Lambda}{8\pi G} \sum_{s \in \mathcal{T}} V_s \tag{6}$$

where h represents the $(d-1)$-dimensional hinge where curvature is concentrated with deficit angle δ_h[7] and s represents the $(d+1)$-dimensional simplex which means the second sum is just the volume of spacetime[8], and Hartle and Sorkin demonstrated [5] that Gibbons-Hawking-York boundary term in Regge Calculus assumes the form

$$S^{(R)}_{GHY}[\mathcal{T}] = \frac{1}{8\pi G}\sum_{h\in\partial\mathcal{T}} V_h\psi_h \tag{7}$$

where h represents the $(d-1)$-dimensional hinge in the boundary $\partial\mathcal{T}$ with deficit angle ψ_h.[9]

We now have to turn these sum into the framework of CDT which uses connectivity. We will just state the results without proofs and refer readers to [2][3][8][11] for the complete proofs of these results ($(2+1)$ case),

$$\begin{aligned} S^{(R)}_E = \frac{ia}{8\pi G}[&\frac{2\pi}{i}(N_1^{SL} - N_1^{SL}(\mathcal{T}_i) - N_1^{SL}(\mathcal{T}_f)) - \frac{1}{i}\theta^{(2,2)}_{SL}(2N_3^{(2,2)} - N^{(2,2)}_{3\uparrow}(\mathcal{T}_i) - N^{(2,2)}_{3\downarrow}(\mathcal{T}_f)) \\ &- \frac{1}{i}\theta^{(1,3)}_{SL}(4N_1^{SL} - 2N_1^{SL}(\mathcal{T}_i) - 2N_1^{SL}(\mathcal{T}_f)) - 2\pi i\sqrt{-\alpha}N_1^{TL} + 4i\sqrt{-\alpha}\theta^{(2,2)}_{TL}N_3^{(2,2)} \\ + 3i\sqrt{-\alpha}\theta^{(1,3)}_{TL}N_3^{(1,3)} &+ 3i\sqrt{-\alpha}\theta^{(3,1)}_{TL}N_3^{(3,1)} + (\frac{2\pi}{i}N_1^{SL}(\mathcal{T}_i) - \frac{4}{i}\theta^{(3,1)}_{SL}N_1^{SL}(\mathcal{T}_i) - \frac{1}{i}\theta^{(2,2)}_{SL}N^{(2,2)}_{3\uparrow}(\mathcal{T}_i) \\ &- \frac{1}{i}\theta^{(2,2)}_{SL}N^{(2,2)}_{3\downarrow}(\mathcal{T}_f))] + \frac{i\Lambda}{8\pi G}[V_3^{(2,2)}N_3^{(2,2)} + V_3^{(1,3)}N_3^{(1,3)} + V_3^{(3,1)}N_3^{(3,1)}] \end{aligned} \tag{8}$$

where θ, N, and V denote Euclidean dihedral angles, number of simplices, and Euclidean volumes of appropriate type of simplicies referred.

3 Results from Causal Dynamical Triangulations

As pointed out in the introduction, CDT has results showing both appropriate semi-classical limit and novel quantum phenomena. Although an individual spacetime history is not a quantum observable, expectation value of the spacetime history of the ensemble and the fluctuations around the expectation are quantum observables. These observables provide a way of exploring semi-classical limit and novel quantum phenomenon.

3.1 Classical Extended Geometry

As it was pointed out briefly, CDT takes Wilsonian approach of adjusting bare constants, $k_0(=\frac{\sqrt{3}a^2}{8G})$ and Δ (which is a constant that measures the asymmetry between the timelike edge length and spacelike edge length), to arrive at a meaningful results. Just like some statistical system, this adjustment of bare constant values give phase structures, where phase transition occurs at some critical value of the constants. When bare constants are appropriately tuned, we arrive at a very special phase C; in $(2+1)$ case with each of time slices being topologically S^2, when initial and final slices have minimal number of triangles required to triangulate S^2, namely 4, we get

[7] Deficit angle δ_h gives a measure of failure of summation of angles around a hinge h to be 2π, namely $2\pi - \sum_{t\ni h}\theta(t,h)$ where $\theta(t,h)$ is the dihedral angle of a $(d+1)$-dimensional simplex around h. This makes sense since we usually think of curvature by parallel transporting a vector around a loop, which does not come back to a same vector if there is a curvature.

[8] Note that Λ can be viewed as a Lagrange Multiplier for fixed spacetime volume.

[9] Since you cannot make a complete loop around the hinge to come back to a same point at the boundary, the deficit angle here is a measure of failure of summation of angles going from one spacelike face to another spacelike face to be π.

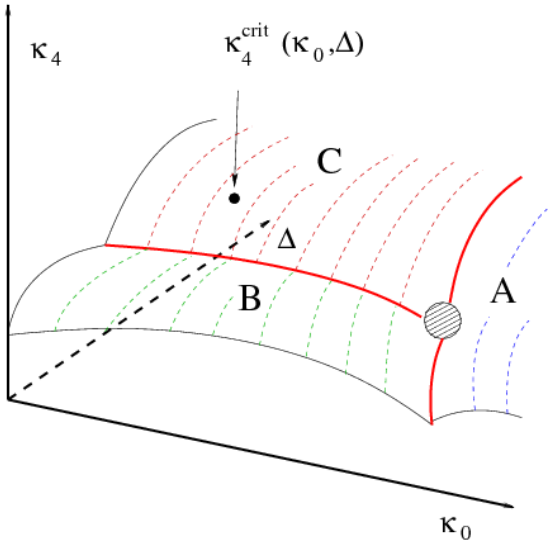

Figure 3.1: Phase structure in $(3+1)$-dimensions.

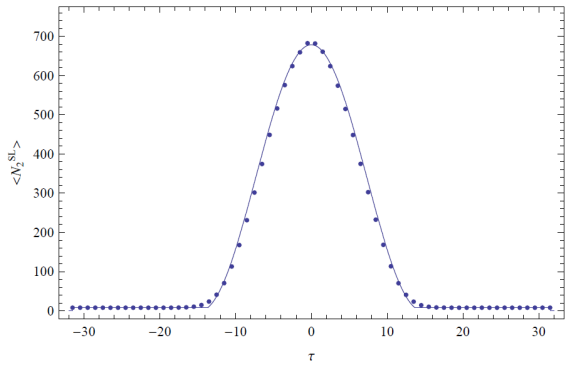

Figure 3.2: Curvefit for Euclidean de Sitter space.

an expectation of spacetime history that resembles a Wick rotated classical General Relativity's solution, Euclidean de Sitter space.

Although such phase C exists in both $(2+1)$ and $(3+1)$, we continue to fix our attention to $(2+1)$.[10] To successfully demonstrate that numerical results resemble the classical solution, we have to discretize the volume profile of the continuous solution. The metric needs to be in 'proper-time' form for the comparison to be made. That is, we turn $V_2(t)$, a 2-volume function over proper-time 't' into $\mathscr{N}_2^{SL}(\tau)$, which is a discretization form of $V_2(t)$ that will be compared with $N_2^{SL}(\tau)$, number of (2)-dimensional simplices at a time slice 'τ'.

A very similar procedure will be used for a derivation for Lorentzian de Sitter volume profile in section 4, therefore we state the result of discretization for Euclidean de Sitter volume profile without proofs,

$$\mathscr{N}_2^{SL}(\tau) = \frac{2}{\pi}\frac{\langle N_3^{(1,3)}\rangle}{\tilde{s_0}\langle N_3^{(1,3)}\rangle^{1/3}}\cos^2\left(\frac{\tau}{\tilde{s_0}\langle N_3^{(1,3)}\rangle^{1/3}}\right) \qquad \text{Euclidean de Sitter} \tag{9}$$

where $\langle N_3^{(1,3)}\rangle$ represents the ensemble average of the number of type $(1,3)$ 3-simplices and $\tilde{s_0}$ represents a parameter to fit numerical result. Figure 3.2 shows how good the fit of the numerical result by equation (9) is.

3.2 Spectral Dimension

Spectral dimension is a way of measuring dimensions at a different scales. The novel quantum mechanical phenomena CDT provides in this area is quite stunning and readers are highly recommended to read more thorough discussions on the topic [2][3][7][8]. When we probe the dimension of $(3+1)$-manifold, classically we obviously expect dimension measurement of the manifold to return 4. However, when we measure the dimension of the expectation value of the spacetime history, we get a dimensional reduction in a smaller scale, and it approaches 4 as we probe larger and larger scale.

[10] Also, simulations for fixed boundary conditions have only been completed for $(2+1)$. $(3+1)$ simulations use periodic boundary condition in which initial and final slices are identified.

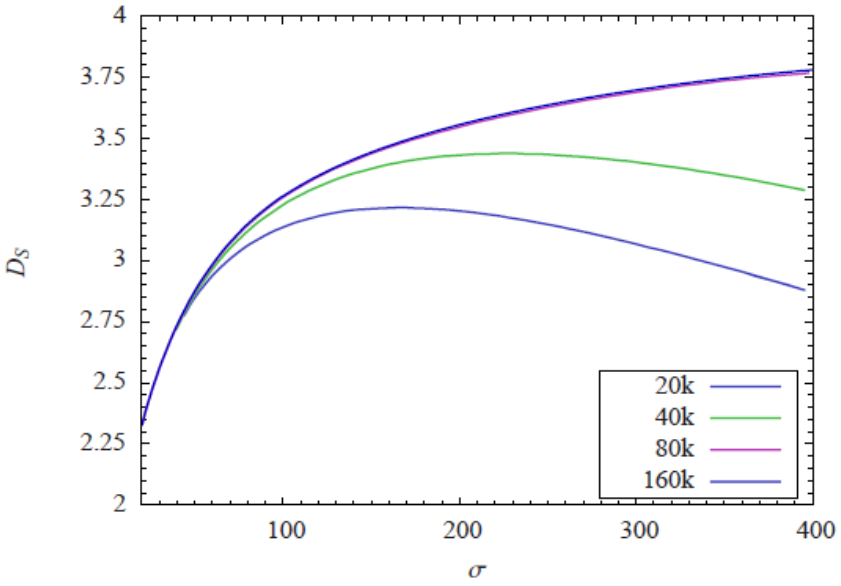

Figure 3.3: Spectral dimension of $(3+1)$ simulation, which approaches 4 as the scale we probe gets larger and larger. The dimensional reduction that happens for some of the curves at a larger scale is due to the finite size of the simulation (as a proof, we see that when we increase the size of the simulation, the dimensional reduction at a larger scale disappears). Image from [2].

4 Lorentzian de Sitter Solution

Throughout this section, we will be discussing in $(2+1)$ frame. As we discussed earlier, when we use minimal number of triangles to triangulate initial and final slices, the volume profile of the simulation closely resembles that of the Euclidean de Sitter solution. However, when we sufficiently increase the number of boundary triangles keeping the total number of 3-dimensional simplices and time slices fixed, we get a volume profile of the simulation that closely resembles that of Lorentzian de Sitter solution.

4.1 Discretizing the Continuous Solution

To test our hypothesis that numerical results matches the volume profile of Lorentzian de Sitter space, we need to discretize the classical solution as previously discussed in the case of Euclidean de Sitter space.

We set out to prove the following discretization result.

$$\mathscr{N}_2^{SL}(\tau) = \frac{2\langle N_3^{(3,1)}\rangle \cosh^2\left(\frac{\tau}{\tilde{s_0}\langle N_3^{(3,1)}\rangle^{1/3}}\right)}{\tilde{s_0}\langle N_3^{(3,1)}\rangle^{1/3}\left(\sinh\left(\frac{S}{\tilde{s_0}\langle N_3^{(3,1)}\rangle^{1/3}}\right) + \frac{S}{\tilde{s_0}\langle N_3^{(3,1)}\rangle^{1/3}}\right)} \qquad \text{Lorentzian de Sitter} \qquad (10)$$

Proof. To begin the proof, we write the metric of Lorentzian de Sitter space in proper-time form, $ds^2 = -g_{tt}dt^2 + l_{ds}^2\cosh^2(\sqrt{-g_{tt}}t/l_{ds})d\Omega_2^2$, where l_{ds} represents de Sitter length and $d\Omega_2^2 = d\theta^2 + \sin^2\theta d\phi^2$.

Lorentzian de Sitter space has a infinite spacetime volume, however, our numerical simulation has fixed spacetime volume. Therefore, we restrict the limits of integration to time interval length 'T':

$$\begin{aligned}
V_3 &= \int_{-\frac{T}{2}}^{\frac{T}{2}} \int_0^{2\pi} \int_{-\pi}^{\pi} \sqrt{g} d\theta d\phi dt \\
&= 4\pi l_{ds}^2 \int_{-\frac{T}{2}}^{\frac{T}{2}} \sqrt{-g_{tt}} \cosh^2(\frac{\sqrt{-g_{tt}}t}{l_d s}) dt \\
&= 2\pi l_{ds}^2 \int_{-\frac{T}{2}}^{\frac{T}{2}} \sqrt{-g_{tt}} (\cosh(\frac{2\sqrt{-g_{tt}}t}{l_{ds}}) + 1) dt \\
&= 2\pi l_{ds}^2 \sqrt{-g_{tt}} (\frac{l_{ds}}{\sqrt{-g_{tt}}} \sinh(\frac{\sqrt{-g_{tt}}T}{l_{ds}}) + T)
\end{aligned}$$

Now we express the 2-volume in terms of 3-volume for given time coordinate value t.

$$\begin{aligned}
V_2 &= 4\pi l_{ds}^2 \cosh^2(\frac{\sqrt{-g_{tt}}t}{l_{ds}}) \\
&= \frac{2V_3 \cosh^2(\frac{\sqrt{-g_{tt}}t}{l_{ds}})}{\sqrt{-g_{tt}}(\frac{l_{ds}}{\sqrt{-g_{tt}}} \sinh(\frac{\sqrt{-g_{tt}}T}{l_{ds}}) + T)}
\end{aligned}$$

Now, we shift our attention to discrete case. We first note that $N_2^{SL} = (N_3^{(1,3)} + N_3^{(3,1)})/2$, since any 2-spacelike simplex is part of one $(3,1)$-simplex and one $(1,3)$-simplex. Also, $N_3 = N_3^{(1,3)} + N_3^{(3,1)} + N_3^{(2,2)}$, which just means total number of 3-simplices is sum of total number of 3-simplices of each kind. Thus, we get the expression, $N_3 = 2(1+\xi) \sum_{\tau=1}^{M} N_2^{SL}(\tau)$ where M represents number of time slices, $N_2^{SL}(\tau)$ represents total number of 2-spacelike simplices on the timeslice τ and $\xi = N_3^{(2,2)}/(N_3^{(1,3)} + N_3^{(3,1)})$.

To relate discrete and continuous case, we have to take continuum limit by taking the lattice spacing $a \to 0$ and total number of 3-simplices $N_3 \to \infty$ while $a^3 N_3$ =constant. In particular, we expect the condition

$$V_3 = C_3 a^3 N_3, \tag{11}$$

where C_3 is the effective discrete spacetime 3-volume of a 3-simplex. Then, if we take a p-dimensional continuous quantity, we expect it to scale like $V_3^{p/3}/N_3^{p/3}$. For instance, $t \propto \tau a \propto \tau V_3^{1/3}/N_3^{1/3}$.

When we use (11), we get

$$\begin{aligned}
V_3 = \int dt \sqrt{g_{tt}} V_2(t) &= 2C_3 a^3 (1+\xi) \sum_{\tau=1}^{M} N_2^{SL}(\tau) \\
\sqrt{g_{tt}} V_2(t) &= 2C_3 a^3 (1+\xi) N_2^{SL}(\tau) \\
N_2^{SL}(\tau) &= \frac{dt V_3 \cosh^2(\frac{\sqrt{-g_{tt}}}{l_{ds}}t)}{(\frac{l_{ds}}{\sqrt{-g_{tt}}} \sinh(\frac{\sqrt{-g_{tt}}T}{l_{ds}}) + T)} \frac{1}{C_3 a^3 (1+\xi)} \\
&= \frac{dt N_3 \cosh^2(\frac{\sqrt{-g_{tt}}}{l_{ds}}t)}{(\frac{l_{ds}}{\sqrt{-g_{tt}}} \sinh(\frac{\sqrt{-g_{tt}}T}{l_{ds}}) + T)} \frac{1}{(1+\xi)}
\end{aligned}$$

We then use $\Delta\tau/N_3^{1/3} = dt/V_3^{1/3}$, $\tau/N_3^{1/3} = t/V_3^{1/3}$, and $S/N_3^{1/3} = T/V_3^{1/3}$ where S is the discrete quantity analog to T.[11] Since $\Delta\tau = 1$,

$$\begin{aligned} N_2^{SL}(\tau) &= \frac{V_3^{1/3} N_3 \cosh^2(\frac{\sqrt{-g_{tt}} V_3^{1/3}}{N_3^{1/3} l_{ds}}\tau)}{N_3^{1/3}(\frac{l_{ds}}{\sqrt{-g_{tt}}}\sinh(\frac{\sqrt{-g_{tt}} V_3^{1/3} S}{N_3^{1/3} l_{ds}}) + \frac{V_3^{1/3}}{N_3^{1/3}} S)} \frac{1}{(1+\xi)} \\ &= \frac{N_3 \cosh^2(\frac{\tau}{s_0 N_3^{1/3}})}{(N_3^{1/3} s_0 \sinh(\frac{S}{s_0 N_3^{1/3}}) + S)} \frac{1}{(1+\xi)} \end{aligned}$$

where $1/s_0 = V_3^{1/3}\sqrt{-g_{tt}}/l_{ds}$. Lastly, we modify our parameter to $\tilde{s_0} = s_0(2(1+\xi))^{1/3}$, which gives

$$N_2^{SL}(\tau) = \frac{2N_3^{(3,1)} \cosh^2(\frac{\tau}{\tilde{s_0}(N_3^{(3,1)})^{1/3}})}{\tilde{s_0}(N_3^{(3,1)})^{1/3}(\sinh(\frac{S}{\tilde{s_0}(N_3^{(3,1)})^{1/3}}) + \frac{S}{\tilde{s_0}(N_3^{(3,1)})^{1/3}})}$$

Since we fit using $\langle N_2^{SL}(\tau)\rangle$, we arrive at the equation,

$$\mathscr{N}_2^{SL}(\tau) = \frac{2\langle N_3^{(3,1)}\rangle \cosh^2(\frac{\tau}{\tilde{s_0}\langle N_3^{(3,1)}\rangle^{1/3}})}{\tilde{s_0}\langle N_3^{(3,1)}\rangle^{1/3}(\sinh(\frac{S}{\tilde{s_0}\langle N_3^{(3,1)}\rangle^{1/3}}) + \frac{S}{\tilde{s_0}\langle N_3^{(3,1)}\rangle^{1/3}})}$$

□

5 CDT with Mass

Due to the lack of local degrees of freedom in $(2+1)$, we want to find a way to model of the universe with mass in $(3+1)$ framework.

Another way to test semi-classical limit in CDT is to create a setting with localized mass (energy). For instance, we can create a setting where two different masses are separated by a fixed distance to see whether it respects Newtonian limits (In General Relativity, such setting creates a strut that has a force that approaches appropriate Newtonian force)[10]. Our attempt is first to create a single spherical mass, which may give a volume profile that resembles that of Wick rotated Schwarzschild de Sitter space. This will also be a test of the classical limit since such solution has many classical applications, such as behavior of light bending around the sun.

5.1 Epp Quasilocal Energy

In General Relativity, physical observables are nonlocal in spacetime, and this includes energy. The best we could do is compute a 'quasilocal energy', an energy that is defined at an extended but finite region of spacetime. There are many different perscriptions of quasilocal energy, but we use Epp quasilocal energy, which is covariant. For the discussion of how Epp quasilocal energy behaves correctly not only in stationary but non-stationary spacetime, refer to [12].

[11] Since T represents time interval length in continuum case, S represents number of thick slices (number of slices bounded by two timeslices), which is $M-1$.

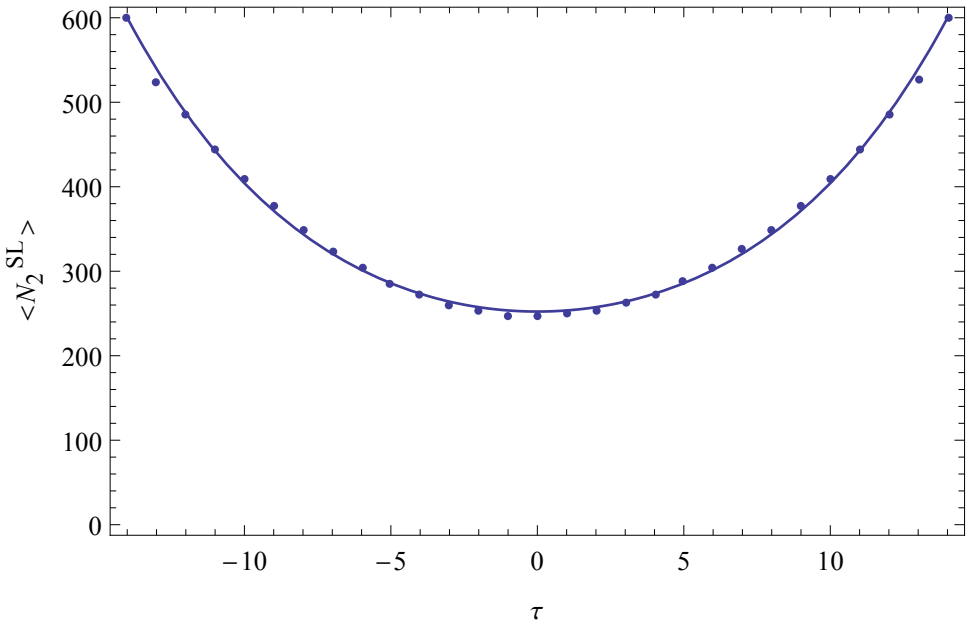

Figure 4.1: A curve fit of numerical simulation with 600 boundary triangles for initial and final slices and 29 timeslices using equation (10). The chi-squared per degree of freedom χ^2_{pdf} was 86.67.

Figure 5.1: If we wish to compute the quasilocal energy of the region R, we consider the extrinsic curvature of its boundary Ω embedded in the spacelike hypersurface Σ and timelike hypersurface B, which is formed by Ω's time evolution. Image from [12].

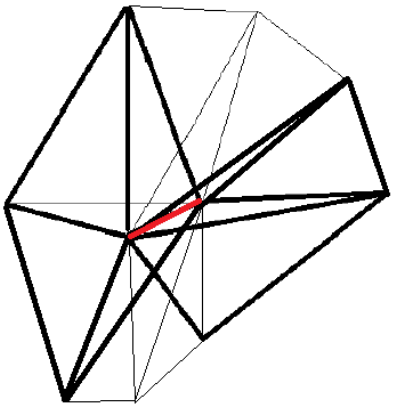

Figure 5.2: A spacelike edge (red) is contained by two $(3,1)$-simplices and two $(1,3)$-simplices. There can be as many future or past-directed $(2,2)$-simplices associated with the edge as the figure shows.

Take a 4-dimensional manifold $\mathscr{M}$ diffeomorphic to $\mathbb{R}\times\Sigma$, where Σ is spacelike 3-dimensional hypersurface. Thus Σ_t represents the leave at 't' of the foliation of $\mathscr{M}$.

Say we wish to compute the quasilocal energy of the finite region R in the hypersurface. The 2-dimensional boundary ∂R (which we label Ω) has two independent embeddings into 3-dimensions, namely its embedding on spacelike hypersurface Σ, and its embedding on timelike hypersurface B, the time evolution of the Ω (you move points of Ω along its integral curve defined by $t^\mu = \partial f^\mu/\partial t$ where f is the diffeomorphism $f : \mathbb{R}\times\Sigma \to \mathscr{M}$). To compute Epp quasilocal energy, we must compute $\frac{1}{8\pi G}\int_\Omega d^2x\sqrt{|\sigma|}k$ and $\frac{1}{8\pi G}\int_\Omega d^2x\sqrt{|\sigma|}l$ where σ is the induced metric on Ω and k and l represent the trace of extrinsic curvature with respect to embedding on Σ and B, respectively.

Now, we imagine how the situation applies in CDT framework. We may want to localize some amount of quasilocal energy in few simplices (say one); we will call this simplex our mass simplex, which we will identically define on every timeslices. We then compute the extrinsic curvature of the mass simplex, which as we will demonstrate involve summing angles around hinges on the mass simplex. Therefore, if we wish to keep the quasilocal energy of the mass simplex fixed throughout the simulation, it involves understanding which neighboring simplices are important in computing the mass simplex's extrinsic curvatures and fixing them throughout the simulation. Some of these fixed neighboring simplices will belong to spacelike hypersurface analogous to Σ above and others will belong to timelike hypersurface analogous to B above.

5.2 Extrinsic Curvature Terms

$\frac{1}{8\pi G}\int_\Omega d^2x\sqrt{|\sigma|}k$ and $\frac{1}{8\pi G}\int_\Omega d^2x\sqrt{|\sigma|}l$ terms we need in order to compute Epp quasilocal energy are not in a discrete form that we can use in CDT framework. As we pointed out earlier in (7), Hartle and Sorkin derived the Gibbons-Hawking-York boundary term, $S_{GHY}[g] = \frac{1}{8\pi G}\int_{\partial\mathscr{M}} d^dy\sqrt{|\gamma|}K$, in Regge Calculus language. Although the expression is derived for the boundary action terms, we note that Gibbons-Hawking-York boundary term looks almost identical to the terms that we need to compute for quasilocal energy.[12]

[12]However, since the hinges around mass simplex that we go around are not in the boundary, unlike the deficit angle in (7), our deficit angle here is the measure of failure of summation of angles around a hinge h to be 2π.

Based on the Wick rotated version of (7), we have

$$\frac{1}{8\pi G}\int_\Omega d^2x\sqrt{|\sigma|}k = \frac{1}{8\pi G}\sum_{h\in\Omega}\frac{a}{i}(2\pi - \theta^3_{SL}N_3^{SL}(h)) \tag{12}$$

where a is the length of the spacelike edge of the mass simplex, θ^3_{SL} is the spacelike dihedral angles[13] of the spacelike 3-dimensional simplex attached to the hinge of the mass simplex, and $N_3^{SL}(h)$ is the number of spacelike 3-dimensioanl simplices attached to the hinge 'h'. Also, $\frac{1}{8\pi G}\int_\Omega d^2x\sqrt{|\sigma|}l = \frac{1}{8\pi G}\sum\limits_{h\in\Omega}\frac{a}{i}(2\pi - 2\theta^{(1,3)}_{SL} - 2\theta^{(3,1)}_{SL} - \theta^{(2,2)}_{SL}N^{(2,2)}_{3\downarrow}(h) - \theta^{(2,2)}_{SL}N^{(2,2)}_{3\uparrow}(h))$ where $\theta^{(a,b)}_{SL}$ represents the spacelike dihedral angle of the timelike (a,b) 3-dimensional simplex. The $N^{(2,2)}_{3\uparrow}(h)$ and $N^{(2,2)}_{3\downarrow}(h)$ are the number of future and past-directed $(2,2)$ simplices attached to the hinge 'h', respectively. Any spacelike edge is contained by two $(3,1)$-simplex and two $(1,3)$-simplex and it can have as many $(2,2)$ simplices in between as the figure 5.2 shows. Since $\theta^{(3,1)}_{SL} = \theta^{(1,3)}_{SL}$ and we can also just write $N_3^{(2,2)}(h) = N^{(2,2)}_{3\uparrow}(h) + N^{(2,2)}_{3\downarrow}(h)$, the equation simplifies to

$$\frac{1}{8\pi G}\int_\Omega d^2x\sqrt{|\sigma|}l = \frac{1}{8\pi G}\sum_{h\in\Omega}\frac{a}{i}(2\pi - 4\theta^{(3,1)}_{SL} - \theta^{(2,2)}_{SL}N_3^{(2,2)}(h)). \tag{13}$$

5.3 Integral Curve

Still the nagging question remains, which neighboring simplices do we need to fix? The spacelike 3-simplices that contains one of the edge of the mass simplex is pretty simple to identify, since our simulation already has a built in foliation with 3-dimensional spacelike hypersurfaces. However, the integral curve of the mass simplex, 3-dimensional timelike manifold is not built into the simulation *a priori*. Therefore, how do we find a right definition of the integral curve of the mass simplex? We are currently testing different definitions of the integral curve, but there are several guidelines that we are using to possibly come up with the right definition of the integral curve, which we will deal with now.[14]

5.3.1 Consistence with Pachner Moves

Pachner moves change triangulation of the manifold, which may remove simplices that previously existed and introduce simplices that previously did not exist. Throughout the simulation, we fix the simplices that are part of integral curve, therefore there is no fear of losing simplices that are part of the integral curve according to the definition we use. However, pachner move may create new simplices that are part of the integral curve according to the definition of the integral curve we use. We say such definition of the integral curve is not consistent with pachner moves, which we may expect from the correct definition of the integral curve.

There are several definitions of integral curves that are not consistent with pachner moves. For instance, if we take timelike 3-simplices (which has its verticies in two slices) that have at least one edge that is part of the mass simplex and have at least one point in each slice being part of mass simplex to form the integral curve, there is a pachner move that will create new simplex that falls into this definition of this integral curve.

[13] An angle formed between two faces of the 3-dimensional simplex around the spacelike edge.

[14] We cannot expect these criterias to absolutely vital, we can merely use them as guidlines to coming with the right definition of the integral curve.

5.3.2 Topology of the Integral Curve

Since the surface of a single simplex has a topology of S^2, and $(3+1)$ uses the perodic boundary condition which gives S^1 topology for time, we may expect the integral curve to have the topology of $S^2 \times S^1$, which is closed. Unfortunately, none of the several integral curve definitions that we considered were topologically closed.

5.3.3 Behavior at the Singularity

Since integral curve is just the time evolution of the surface of the mass simplex, we may try to arrive at the correct definition by brute force. We may imagine timelike vectors on each points of the mass simplex emanating from its face; however, if we evolve each of these points on the mass simplex, most of them meets timelike surface, which has a curvature concentrated to it.[15] The question is, how does the integral curve behave upon encountering such singularity? Exploring the answer to this question may help one to arrive at the correct definition of the integral curve to use.

5.4 Building a Mass Model

One of the definition of the integral curve that we think may be the correct definition, which is also consistent with pachner moves, is taking timelike simplices that have at least one edge that belongs to the mass simplex. With such definition of the integral curve, how do we go about building a model with the mass simplex and all the neighboring fixed simplices identified? This is not so simple. For instance, let us consider the minimal triangulation of the timeslice, which has five 3-dimensional siimplices, which we label its vertices by integers. Since we can repeat our mass building procedures between any two slices, it is sufficient to consider only two slices. On the lower slice then, we have the 3-simplices labeled by (1 2 3 4), (1 2 3 5), (1 2 4 5), (1 3 4 5), and (2 3 4 5). On the upper slice, we have $(1'\ 2'\ 3'\ 4')$, $(1'\ 2'\ 3'\ 5')$, $(1'\ 2'\ 4'\ 5')$, $(1'\ 3'\ 4'\ 5')$, and $(2'\ 3'\ 4'\ 5')$. These are then connected by timelike edges to form 4-dimensional simplices, namely, $(1\ 2\ 3\ 4 \mid 1')$, $(1\ 2\ 3\ 5 \mid 2')$, $(1\ 2\ 4\ 5 \mid 3')$, $(1\ 3\ 4\ 5 \mid 4')$, $(2\ 3\ 4\ 5 \mid 5')$, $(1 \mid 1'\ 2'\ 3'\ 4')$, $(2 \mid 1'\ 2'\ 3'\ 5')$, $(3 \mid 1'\ 2'\ 4'\ 5')$, $(4 \mid 1'\ 3'\ 4'\ 5')$, $(5 \mid 2'\ 3'\ 4'\ 5')$, $(1\ 2\ 3 \mid 1'\ 2')$, $(1\ 2\ 4 \mid 1'\ 3')$, $(1\ 3\ 4 \mid 1'\ 4')$, $(2\ 3\ 4 \mid 1'\ 5')$, $(1\ 2\ 5 \mid 2'\ 3')$, $(1\ 3\ 5 \mid 2'\ 4')$, $(2\ 3\ 5 \mid 2'\ 5')$, $(1\ 4\ 5 \mid 3'\ 4')$, $(2\ 4\ 5 \mid 3'\ 5')$, $(3\ 4\ 5 \mid 4'\ 5')$, $(1\ 2 \mid 1'\ 2'\ 3')$, $(1\ 3 \mid 1'\ 2'\ 4')$, $(1\ 4 \mid 1'\ 3'\ 4')$, $(1\ 5 \mid 2'\ 3'\ 4')$, $(2\ 3 \mid 1'\ 2'\ 5')$, $(2\ 4 \mid 1'\ 3'\ 5')$, $(2\ 5 \mid 2'\ 3'\ 5')$, $(3\ 4 \mid 1'\ 4'\ 5')$, $(3\ 5 \mid 2'\ 4'\ 5')$, and $(4\ 5 \mid 3'\ 4'\ 5')$, where '|' denotes the separation of the vertices in the lower and upper slices (and yes, this is only the minimum triangulation).

Now, to see what 3-dimensional timelike simplices we have (and we will not list them all here), we need to take a 4-dimensional simplex and look at its 3-dimensional subsimplices just by taking 4 of its vertices. For instance, $(1\ 2\ 3\ 4 \mid 1')$ has following 3-dimensional subsimplices, of which only one of them are spacelike: (1 2 3 4), $(1\ 2\ 3 \mid 1')$, $(1\ 2\ 4 \mid 1')$, $(1\ 3\ 4 \mid 1')$, $(2\ 3\ 4 \mid 1')$. Since a pachner move changes subsimplices around, if a 4-dimensional simplex contains one of the fixed 3-dimensional subsimplex, we have to fix 4-dimensional simplex that contains the fixed 3-dimensional subsimplex. Now, let us without loss of generality, assume that (1 2 3 4) is our mass simplex. If we use the integral curve definition we just introduced, every single one of our 4-dimensional simplices become fixed, therefore simulation is doomed. Therefore, we need to implement few initial moves to have more than minimal triangulation of the timeslice before assigning mass simplex, such that not every simplices are frozen.

[15] Recall that in (n)-dimensional manifold, curvatures are concentrated in $(n-2)$-dimensional subsimplices

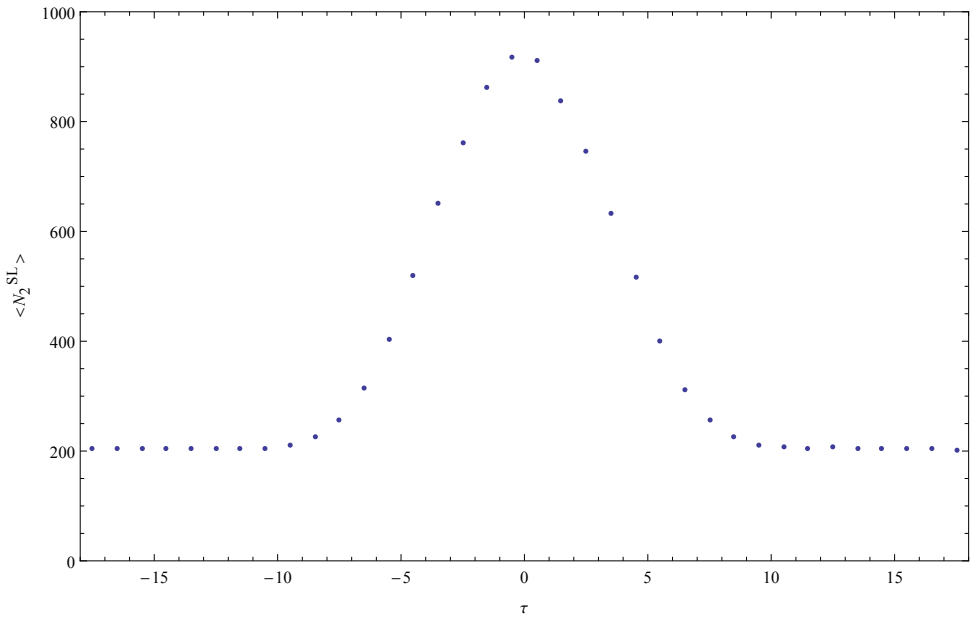

Figure 5.3: Mass simulation with total number of 4-simplices and timeslices as 40464 and 37, respectively. We used the integral curve definition introduced in Section 5.4, and this particular model has around 180 3-simplices fixed in each slices.

It is reasonable to expect the correct mass model should be able to make any type of the pachner moves. We have developed a Python program that tracks all the simplices information while making a desired pachner move on a desired simplicial complex. We were able to create a symmetrical mass model under the integral definition we specified in the beginning, such that there are enough free simplices to allow every type of the pachner moves. We also developed an algorithm to create a mass model to allow mass to have an arbitrarily high quasilocal energy. The program also tests the topology information of the integral curve, and facilitates the investigation of the validity of the different definitions of the integral curve. The model that we created has a very long list of simplices, which we will refrain from writing down on this paper.

5.5 Results and Outlooks

We have modified the $(3+1)$ CDT Simulation code written in Common LISP by R. Kommu to allow specified simplices to be fixed throughout the simulation to test our mass model. According to the paper [9], the point-like mass (localized mass within a single simplex like the one we created) should give the volume profile of Euclidean Schwarzschild de Sitter space. As we always have in other cases, the volume profile must be derived using proper-time metric form. The problem is, however, in Euclidean Schwarzschild de Sitter space, proper-time coordinate does not cover the entire manifold. Therefore, we excise the mass region, and focus our attention in the exterior vacuum region. However, if the mass becomes too large, the caustic region (which lies within the mass region otherwise) extend to the exterior vacuum region. Therefore, the paper argues that mass has an upperbound, and the low mass allows the volume profile of Euclidean Schwarzschild de Sitter to be seen as a perturbation of the volume profile of Euclidean de Sitter space. Our preliminary result of the simulation with the integral curve definition introduced in the previous subsection has a volume profile that definitely resembles that of Euclidean de Sitter space. We are currently testing other definitions of the integral curve to see whether we really

landed on the right integral curve definition.

Eventually, we hope that we can also create a situation with two mass model to further test our Newtonian limits as discussed earlier in the section. Another project one can work on is constructing the phase structure with mass simplex.

Acknowledgements

I would like to thank Professor Steve Carlip, for making this research possible and for many helpful discussions. Also, I would like to thank Joshua Cooperman, for his amazing patience and guidance along every step of the way of the research project. The project was funded by Chapman University's SURF program and also would not have been possible without the hospitality of UC Davis's Physics Department.

References

[1] J. Ambjørn, A. Görlich, J. Jurkiewicz, and R. Loll. "Nonperturbative quantum de Sitter universe." *Physical Review D* 78 (2008) 063544.

[2] J. Ambjørn, A. Görlich, J. Jurkiewicz, and R. Loll. "Nonperturbative quantum gravity." *Physics Reports* 519 (2012) 127.

[3] J. Ambjørn, J. Jurkiewicz, and R. Loll. "Dynamically triangulating Lorentzian quantum gravity." *Nuclear Physics B* 610 (2001) 347.

[4] J. B. Hartle and S. W. Hawking. "Wave function of the Universe." *Physical Review D* 28 (1983) 2960.

[5] J. B. Hartle and R. Sorkin. "Boundary Terms in the Action for Regge Calculus." *General Relativity and Gravitation* 13 (1981) 541.

[6] T. Regge. "General Relativity without Coordinates." *Nuovo Cimento* 19 (1961) 558.

[7] R. Kommu. "An Investigation of the Causal Dynamical Triangulations Approach to Quantizing Gravity." PhD Dissertation.

[8] J. Cooperman "Exploring Causal Dynamical Triangulations." PhD Dissertation.

[9] I. Khavkine, R. Loll and P. Reska. "Coupling a point-like mass to quantum gravity with causal dynamical triangulations." *Classical and Quantum Gravity* 27 (2010) 185025.

[10] Amnon Katz. "Derivation of Newton's Law of Gravitation from General Relativity." *Journal of Mathematical Physics* 9 (1968) 983.

[11] J. Cooperman and J. Miller. "A first look at transition amplitudes in $(2+1)$-dimensional causal dynamical triangulations."

[12] M. M. Afshar. "Quasilocal Energy in FRW Cosmology." *Classical and Quantum Gravity* 26 (2009) 225005.

[13] R. J. Epp "Angular momentum and an invariant quasilocal energy in general relativity." *Physical Review D* 62 (2000) 124018

[14] C. W. Misner, K. S. Thorne, and J. A. Wheeler. "Gravitation." *W. H. Freeman and Company* (1973).

[15] S. M. Carroll. "Spacetime and Geometry." *Addison Wesley* (2004).

[16] J. M. Miller. "Fixing the Boundaries for Causal Dynamical Triangulations in 2+1 Dimensions." (2012).